CHALMERS
UNIVERSITY OF TECHNOLOGY

Polydopamine/graphene oxide coatings loaded with tetracycline and green Ag nanoparticles for effective prevention of biofilms

Applied Surface Science 626 (2023) 157221

Contents lists available at ScienceDirect

Applied Surface Science

journal homepage: www.elsevier.com/locate/apsusc

Full Length Article

Polydopamine/graphene oxide coatings loaded with tetracycline and green Ag nanoparticles for effective prevention of biofilms

Jian Zhang [a], Priyanka Singh [b], Zhejian Cao [a], Shadi Rahimi [a], Santosh Pandit [a,*], Ivan Mijakovic [a,b,*]

[a] Systems and Synthetic Biology Division, Department of Biology and Biological Engineering, Chalmers University of Technology, SE-412 96 Gothenburg, Sweden
[b] The Novo Nordisk Foundation, Center for Biosustainability, Technical University of Denmark, DK-2800 Kogens Lyngby, Denmark

ARTICLE INFO

Keywords:
Graphene oxide
Ag nanoparticles
Tetracycline
Polydopamine
Antibiofilm coatings

ABSTRACT

Bacterial adhesion and biofilm formation are significant challenges for medical devices and implants. Surface modification to alter the surface properties of biomedical device surfaces to prevent the biofilm formation is an important driving force for the development of anti-biofilm coatings. Here, a simple and feasible method to fabricate antibacterial coatings that combines the adhesion properties of polydopamine (PDA) and the high drug loading capacity of graphene oxide (GO). Tetracycline and green-synthesized silver nanoparticles were successfully assembled onto the coating surface, endowing the coating an anti-biofilm effect and exhibit strong inhibitory effect on *S. aureus* and *E. coli* biofilms by a factor of more than 1000 (3 $\log_{10}$ units). Kirby-Bauer diffusion test, colony forming unit (CFU) counts, biofilm topography studies and live/dead staining were used to evaluate the antibacterial activity of the coatings. This study is proposed that PDA/GO coatings loaded with antibiotics or silver nanoparticles can be used as a potential approach to prevent infection associated with implantable biomedical devices.

1. Introduction

Biofilm are considered a key factor over 65% of nosocomial infections and 80% of all microbial infections.[1] Microbial cells in biofilms adhere to each other and are surrounded by a self-produced extracellular polymeric matrix (EPS). Bacterial cells in biofilms are highly resistant to antibiotics compared to planktonic bacteria. EPS slows the penetration of antibiotics and causes their enzymatic degradation, which is considered a major cause of antimicrobial resistance.[2,3] An important challenge for medical devices and biomedical implants is the adhesion and colonization of pathogens, which in turn forms resilient biofilm infections. This often results in implant failure, patient suffering, and financial loss.[4] Hence, biofilms have been recognized as important targets for bacteriostatic and antibacterial therapy.[3,5,6] Three main strategies have been used to combat biofilms: (1) surface modification technology to prevent bacterial adhesion and colonization; (2) delivery of pharmaceutical systems to penetrate biofilms and kill bacteria by releasing loaded drugs; (3) physical removal of biofilm extracellular polymers to disrupt biofilm habitat. There is a significant drive to develop antibiofilm coatings by surface modification to alter the surface properties of biomedical device surfaces and prevent or minimize bacterial adhesion and growth. A variety of coatings have been developed to render biomedical devices surfaces anti-infective, where nanomaterials have shown great opportunities for the development of antibiofilm coatings.[7–10].

Graphene is a two-dimensional carbon network composed of sp^2-hybridized carbon atoms. Due to its excellent electrical, mechanical, and photothermal properties, graphene has been extensively studied in research fields such as biosensing and energy conversion.[11,12] In addition, the antibacterial activity of graphene-based coatings has also been reported.[13–15] The bacteria are physically punctured and killed directly by the sharp edges exposed by the graphene aligned vertically on the substrate surface. The bacteria can hardly develop resistance to this killing mechanism. Graphene oxide (GO) is a derivative of graphene, and has various functional groups including epoxy, hydroxyl, and carboxyl. In addition, GO is easy to modify and has good chemical stability and dispersibility in water.[16,17] GO materials with antibacterial effects have been attracting increased attention. Similar to graphene, GO can kill bacteria by a direct contact with the sharp edges, which leads to irreversible cellular damage.[18] In addition, bacteria

* Corresponding authors.
E-mail addresses: pandit@chalmers.se (S. Pandit), ivan.mijakovic@chalmers.se (I. Mijakovic).

https://doi.org/10.1016/j.apsusc.2023.157221
Received 20 December 2022; Received in revised form 18 March 2023; Accepted 5 April 2023
Available online 9 April 2023

can be killed by oxidative stress, caused by reactive oxygen species (ROS) produced by GO.[19,20] Besides its direct antibacterial activity, GO can be used as an effective nanocarrier, loaded with antibiotics or other drugs, to achieve drug delivery and release.[21–24].

Dopamine, belonging to the class of catecholamines, can self-polymerize and spontaneously deposit on almost any object as a polydopamine (PDA) film, which makes it a good material for functional coating applications.[25] It has been widely recognized that PDA-coated surfaces can improve the stability of nanoparticles, GO, enzymes, and other materials.[26–28] PDA assisted GO coatings have also been reported.[29] The excellent adhesive properties of PDA can help GO to firmly attach to the substrate during the process of dopamine polymerization. In addition, the secondary amine group on PDA can form an amide group with the carboxyl group of GO and form hydrogen bonds with hydroxyl groups, so that GO can be stably attached to the surface of polydopamine.[30].

In addition to antibiotics, silver nanoparticles (AgNPs) have emerged as the promising anti-infection agents.[31] There is an increasing number of studies using plants or microorganisms for "green synthesis" of biocompatible and environmentally safe AgNPs.[32,33] Unlike AgNPs produced by chemical synthesis, "green" AgNPs contain a corona layer wrapped on their surface. The corona can greatly reduce the AgNPs toxicity, improve the stability and biocompatibility, facilitate internalization in living cells (crossing the membrane), and improve the antibacterial effect.[34] In addition, surface-active functional groups of nanoparticles can be used to immobilize various biomolecules, and there is also great potential in the field of drug delivery and human medical applications.

Antimicrobial materials based on AgNPs, graphene oxide and PDA materials have been investigated previously. For example, AgNPs were synthesized on GO using a chemical reduction method to build nanocomposites.[35] AgNPs were synthesized in situ on the PDA functionalized GO surface, where PDA acted as a reducing agent. The nanocomposites exhibited excellent antibacterial properties.[35–37] PDA/GO coating was self-assembled onto the cellulose membrane by vacuum-assisted filtration and exhibited excellent antibacterial efficiency against both *Staphylococcus aureus* and *Escherichia coli*.[38] However, compared with previously studied GO nanocomposites, there are only few studies on the construction of antimicrobial coatings via GO and PDA. Combating biofilms on coated surfaces is more challenging than inhibiting planktonic bacteria. The anti-biofilm coatings in this study are fabricated by layer-by-layer assembly. Our coatings benefit from a synergy of adhesion properties of PDA, high loading efficiency of GO, and the activity of incorporated antimicrobial agents. The PDA functionalized substrate surface can interact with GO to obtain PDA/GO coatings for the immobilization of two kinds of antimicrobial agents: commercially available tetracycline hydrochloride (TC) and home-made AgNPs obtained by "green synthesis" from *Pseudomonas putida* extracts.[39] The reported coatings are universal and can be easily applied to a wide variety of substrates. The anti-biofilm activity of the coatings was evaluated against biofilms of the opportunistic pathogens *Staphylococcus aureus* and *Escherichia coli*. Our results demonstrate that the coating obtained by immobilizing antimicrobial agents through the PDA/GO layer is highly effective against pathogenic biofilms.

2. Experimental sections

2.1. Bacterial strains, chemicals, and materials

Ultra-highly concentrated GO was obtained from the Graphene supermarket (USA). Dopamine hydrochloride and tetracycline hydrochloride were purchased from Sigma-Aldrich (Sweden). The *Escherichia coli* (*E. coli*) UTI89 and *Staphylococcus aureus* (*S. aureus*) CCUG10778 were used to evaluate the anti-biofilm activity.

2.2. Coating preparations

15 mm diameter coverslip glasses were cleaned by acetone, ethanol, and ultrapure H_2O in order and dried with N_2 flow. PDA/GO coating on glass was performed in batches using Petri dishes containing one concentration and volume of dopamine and GO. The same volume and concentration of AgNPs and TC were incubated on the PDA/GO surface to obtain PDA/GO/TC and PDA/GO/Ag coatings. Glass slides surface were first coated with PDA. It was immersed in Tris buffer (10 mM, pH 8.5) containing 2 mg/mL dopamine hydrochloride for 24 h at room temperature with gentle shaking. Then, the surfaces were washed with ultrapure H_2O for 5 min under sonication, rinsed with a stream of H_2O, and dried with a N_2 flow. The surface coatings were named PDA.

Immobilization of GO on the surface was achieved by immersing the PDA-coated surfaces in GO (1.0 mg/mL) aqueous solution for 16 h at 50 °C. The slides were cleaned with ultrapure H_2O and then baked at 150 °C for 2 h. The surface coatings were named PDA/GO.

Immobilization of TC on the PDA/GO surface was achieved by immersing the PDA/GO samples in 1 mL of TC solution of different concentration (0.5, 1 and 2 mg/mL) for 24 h at 4 °C. And then thoroughly washed with H_2O, dried with a N_2 flow, and transferred to sterile petri dish for further experiments. The coatings are named as PDA/GO/$TC_{0.5}$, PDA/GO/TC_1 and PDA/GO/TC_2 meaning that the assembled concentration of TC is 0.5, 1 and 2 mg/mL, respectively.

A previously reported green method was used for the synthesis of silver nanoparticles (AgNPs).[39] Immobilization of AgNPs on the PDA/GO surface was achieved by immersing PDA/GO slides in a polydiallyldimethylammonium chloride (PDDA) solution (2 mg/mL) for 2 h, rinsed with H_2O, and then dried under N_2. The PDDA modified PDA/GO slides were coated with 300 μL of AgNPs at various concentrations of 13.5, 27, 54, and 108 μg/mL for overnight. And then thoroughly washed with H_2O, dried with a N_2 flow, and transferred to sterile petri dish for further experiments. The coatings are named as PDA/GO/$Ag_{13.5}$, PDA/GO/Ag_{27}, PDA/GO/Ag_{54} and PDA/GO/Ag_{108} meaning that the assembled concentration of AgNPs is 13.5, 27, 54, and 108 μg/mL.

2.3. Characterization of coatings

The surface topography of coatings was monitored using atomic force microscopy (AFM, NT-MDT Spectrum Instruments, Russia). Tests were recorded in semi-contact mode with images at 512 × 512 pixels at a scan rate of 0.5 Hz.

Attenuated total reflectance Fourier-transform infrared (ATR-FTIR) was recorded on Bruker's Alpha spectrometer using diamond crystal as the refractive element. Spectra were acquired from the average of 256 scans at a resolution of 4 cm^{-1}.

Raman spectra were recorded using a WITec alpha300 confocal Raman spectrometer with 100 × objective, 532 nm laser and 600 g/mm grating. Spectra were acquired from the range 500–3000 cm^{-1} and 0.5 s integration time.

The surface chemistry was studied by means of a PHI VersaProbe III X-ray photoelectron spectroscopy (XPS) instrument using monochromatized Al Kα (1486.6 eV) X-ray source. The take-off angle was 90° relative to the surface. The data analysis was performed with CasaXPS software.

The UV–Vis spectrum was acquired on an Agilent Cary 60 spectrophotometer in the range of 300–800 nm. Dynamic light scattering (DLS) (Zetasizer Nano ZS, Japan) was used to study the zeta potential of Ag nanoparticles. Nanoparticles were analyzed for shape and size by transmission electron microscopy (TEM), using a FEI Tecnai T20 G2 instrument operating at 200 kV.

2.4. Antibiofilm assays

The zone of inhibition in Kirby-Bauer disk diffusion test was performed to assess the antimicrobial activity of the coatings. The

experiments were performed with PDA, PDA/GO, PDA/GO/TC, PDA/GO/Ag coatings. Each coating was addressed in one quadrant of the agar plate with *S. aureus* or *E. coli*, which were incubated at 37 °C for 96 h. The diameters of the zone of inhibition were measured every 24 h.

For the antibiofilm assay activity studies, one very common pathogen was selected from the group of Gram-negative (*E.coli*) and Gram-positive (*S. aureus*) bacteria.[40,41] Infections caused by *E.coli* and *S. aureus* pose a serious threat to human health. *S. aureus* is mainly responsible for food poisoning, toxic shock syndrome, endocarditis and postoperative wound infection. *E. coli* is present in the human gut and can cause urinary tract infections, colonic bursitis, or sepsis. In addition, they are also prone to multidrug resistance to antibiotics.

The coatings were evaluated for biofilm inhibition properties against *S. aureus* and *E. coli*. Bacteria grown overnight were diluted in nutrient medium for obtaining the final inoculum of 2–5 $\times$ 10^6 CFU/mL. A 250 μL volume of the inoculum was inoculated onto the coatings and incubated statically at 37 °C to form a biofilm. After 24 h, the inoculum was removed and the coating was rinsed with sterile H_2O to wash the loosely attached bacterial cells. Then, the biofilms were collected from the coatings in 5 mL of 0.89% NaCl buffer and homogenized by sonication. The homogenized biofilm suspension was serially diluted into 0.89 % NaCl and plated on agar plates. After incubation at 37 °C for 24 h, the number of colonies was counted.

The morphology change of biofilms were studied by scanning electron microscopy (SEM). The *S. aureus* and *E. coli* biofilm formed on coatings were fixed using 3% of glutaraldehyde for 2 h. Then, the coatings were dehydrated using graded ethanol (40%, 50%, 60%, 70%, 80%, 90% and 100%) for 20 min. Dried dehydrated biofilms were imaged on a SEM (JEOL 7800F Prime). Biofilms were stained with SYTO 9 and potassium iodide (Live/Dead BacLight Viability kit L13152) and were imaged on a fluorescence microscope (Zeiss Axio Imager Z2m, Germany).

To assess long-term potential of coatings to inhibit biofilm formation, biofilms were grown on the coatings for 3 days. A volume of suspension containing the bacterial inoculum was inoculated on the coatings, which were incubated at 37 °C for 3 days. The culture medium was replaced at 24 h intervals. The biofilms for each day were collected and homogenized and plated on agar plates to count the colonies.

2.5. TC release assessment

To test the TC release from the coatings, the coated matrix was placed to a capped tube containing 1 mL of phosphate-buffered saline (pH 7.4) at 37 °C to allow 24 h of release of TC. The buffer was collected and freshly buffer added every 24 h until 5 days. The collected buffers were quantified by using UV–Vis spectrum. TC concentration calibration curve was established using serially diluted TC solutions ranging from 0.001 to 0.1 mg/mL.

2.6. Biocompatibility

Huh7 human hepatoma cell line was used for this study. The bare glass, PDA/GO, PDA/GO/TC_1, PDA/GO/Ag_{108} coatings samples were kept on 24 well plates and cells at a density of 8 $\times$ 10^4 cells per well were seeded onto 24-well plates and cultured for 24 h. Then, the cells were incubated with medium containing 1 $\times$ alamarBlue (Thermo Scientific) staining solution for 3 h. The signal from the cells was detected using an OPTIMA BLUE Fluostar plate reader (BMG Labtech, Ortenberg, Germany) and the results were normalized to the medium control.

2.7. Statistical analysis

All measurements were performed in triplicate and all data are expressed as mean ± standard deviations. A one-way analysis of variance (ANOVA) with a post hoc multiple comparison (Tukey) test was used. P-value < 0.05 was considered statistically significant.

3. Results and discussions

3.1. Surface characterization of the PDA/GO/TC and PDA/GO/Ag coatings

PDA/GO/TC and PDA/GO/Ag coatings were prepared by layer-by-layer assembly. Atomic force microscopy (AFM) images showed the topography of the coatings. The SEM images of the coatings are shown in **Figure S1.** Surface features of bare glass surface were generally flat and smooth, with the root mean square (rms) roughness values of 0.28 nm (Fig. 1**a**). After PDA formation on the surface (Fig. 1**b**), differences in the surface morphology were observed with typical small polydopamine aggregates appearing on the surface with increased rms roughness to 0.95 nm.[42] After the GO assembly on PDA, the surface rms roughness slightly increased to 1.23 nm due to the presence of GO nanosheets. The surface of the PDA/GO coating shows the presence of GO sheets, as shown by the irregular tile-like features in Fig. 1**c**. GO attachment on the PDA surface can occur via the cross-linking reaction of the secondary amine group on PDA with carboxyl group on GO or via hydrogen bonding interactions with the hydroxyl group on GO.[30,43] After TC was loaded onto the GO, the morphology of the coatings did not change significantly (Fig. 1**d**), and the shape of the coating is not affected by the TC concentration. The self-assembly of AgNPs onto the GO surface is aided by the cationic polyelectrolyte poly(diallyldimethylammonium chloride) (PDDA). The morphology and rms roughness of the PDDA-modified GO surface did not change significantly (Fig. 1**e**). This may be due to the small amount of PDDA modified on GO.[44] The size range of AgNPs is 15–40 nm. The surface of AgNPs is negatively charged, which could be effectively adsorbed on the surface of cationic polymer PDDA. TEM images, Zeta potential, and UV–Vis spectrum results of AgNPs are shown in the supplementary materials (Fig. S2-4). After assembly of AgNPs, the rms roughness of the coating surface was found to increase to 11 nm, and a large number of nanoparticles were observed (Fig. 1**f**), which is consistent with the TEM images results.

Raman spectroscopy was performed to assess the level of "disorder" in the sp^2 hybrid structure of the prepared functionalized materials.[45] The Raman spectra of glass, PDA, PDA/GO, PDA/GO/TC and PDA/GO/Ag coatings are shown in Fig. 2. The Raman spectra of bare glass is assigned to the Si-O stretching vibration.[46] After PDA coating, the bands of glass were disappeared instead of the main band features of the sp^2 carbon material. The G band (1585 cm^{-1}) is attributed to the in-plane vibrations of sp^2 bonded carbon atoms, while the D band (1350 cm^{-1}) is attributed to the out-of-plane vibrations. The relative signal intensities (ID/IG) of the D and G bands provide information to assess the surface defect density of carbon materials.[47] PDA coating showed two bands at about 1358 and 1588 cm^{-1} that are associated to the stretching vibration and deformation of catechol groups. The D and G typical bands for the graphene derivatives overlap with the PDA.[48] However, higher intensity D and G bands (ID/IG) were observed when GO was assembled on PDA, which may be due to the increased defects on GO and the formation of new chemical bonds between GO and PDA.[48] For the PDA/GO/TC and PDA/GO/Ag coatings, the ID/IG is lower than that of PDA/GO, which may be because the TC and AgNPs loaded on GO cover some defects on the surface. For all the GO loaded coatings, weak 2D peak at about 2700 cm^{-1} was observed, confirming the multilayered state of the GO flakes.[49].

XPS was performed to characterize the elemental composition and molecular structure of coatings. Fig. 3**a** shows full XPS spectra of bare glass, PDA, PDA/GO, PDA/GO/TC and PDA/GO/Ag coatings. The atomic percentages of PDA, PDA/GO, PDA/GO/TC and PDA/GO/Ag coatings are shown in **Table S1**. Besides the expected Si, O, Na, Ca and K peaks, a C1s peak is observed in the bare glass sample due to the adsorption of hydrocarbon impurities.[50] The surface elements of PDA coating contains only three elements: C, N, and O. The intensity of the C1s peak is significantly increased, which indicates that the surface of bare glass is successfully coated with a PDA coating. In the spectrum of

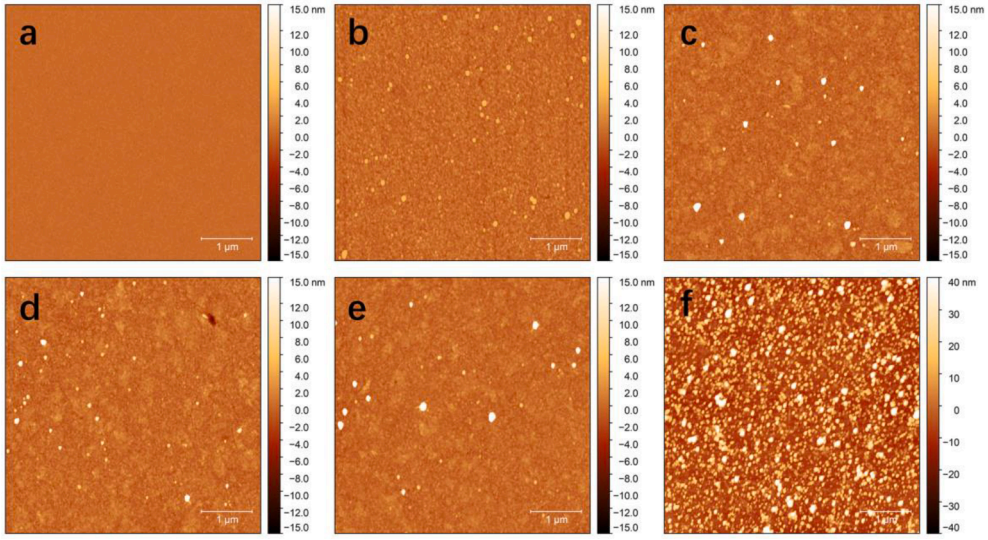

Fig. 1. AFM morphologies of bare (a), PDA (b), PDA/GO (c), PDA/GO/TC (d), PDA/GO/PDDA (e) and PDA/GO/PDDA/Ag (f) coatings with a scanning area of 5 × 5 μm.

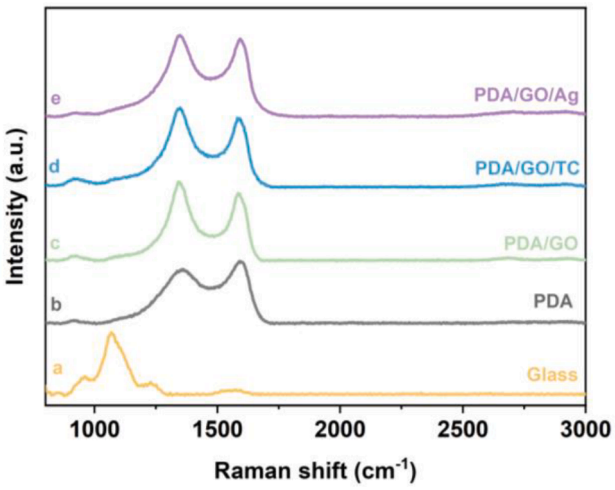

Fig. 2. Raman spectra of PDA (a), PDA/GO (b), PDA/GO/TC (c) and PDA/GO/Ag (d) coatings.

the PDA/GO coating, the intensity of N1s decreased and that of C1s increased compared to PDA, indicating successful GO assembly. In the spectrum of PDA/GO/Ag coating, the appearance of Ag peak clearly indicated the successful assembly of AgNPs.

Peak fitting of high-resolution spectra of C1s can be used to study the chemical state of layer-by-layer coating formation. The C1s spectra of PDA coating could be deconvoluted into components with binding energies at 284.6, 285.8, 287.2, 288.6, and 290.7 eV which are assigned to C–C, C-N, C-O, O = C, and π-π bonds, respectively (Fig. 3**b**).[51,52] As to PDA/GO coating, the C1s spectra could be deconvoluted into different components at 284.6, 285.7, 286.8, 288.5, and 289.8 eV, which correspond to the aromatic C–C, C-N, C-O, O = C, and O = C-O bonds, respectively (Fig. 3**c**). The ratio for oxygen-containing groups increases from 14.85 % to 27.13 % while the ratio for C-N bond decreases from 28.48 to 13.71 %. This is mainly attributed to the fact that the GO sheets were assembled on the PDA surfaces. In addition, GO is reported to be partially reduced due to the polydopamine coating. [23,48] Upon PDA/GO/TC coating, the ratio for C-N bond increases from 13.71 to 23.38 % (Fig. 3**d**). It indicated the successful assembly of TC. Additionally, after AgNPs assembled on PDA/GO surface, the contributions of deconvoluted C1s peaks maybe partially result from the biological corona on the surface of nanoparticles (Fig. 3**e**).[53,54] Fig. 3**f** shows the core level spectrum of Ag3d, the signals at binding energies of 367.89 and 374.08 eV were ascribed to the $Ag3d_{5/2}$ and $Ag3d_{3/2}$ of metallic silver.[55] The high resolution of spectra of O1s results are shown in the supplementary materials (**Figure S5**).

The assembly of TC and AgNPs on GO was indicated by FTIR spectra. As shown in Fig. 4**a**, GO exhibits the following characteristic features: the peak at 1619 cm^{-1} corresponds to the stretching vibration of C = C in the unoxidized graphitic domain, and the stretching vibration of carboxyl C = O and bending vibration of O–H in the oxidized surface domain are evident at 1731 and 1388 cm^{-1}, respectively. The band at 1053 cm^{-1} corresponds to the stretching vibration of C-O group, while the broad band at 3369 cm^{-1} corresponds to the –OH vibration stretching.[56] The spectrum of free TC shows absorption band at 3380 cm^{-1} attributed to O–H stretching. The bands at 1648 and 1582 cm^{-1} are characteristic of amide carbonyl and carbonyl groups. The bands at 1448 and 1227 cm^{-1} are characteristic of C = C (aromatic ring) and N–H bonds, respectively.[57] After TC was assembled on GO, there was no characteristic peak at 1731 cm^{-1} in the spectrum. However, bands at 1581, 1454 and 1226 cm^{-1} correspond to C = O vibration of amide, and C = C vibration of TC aromatic ring.[21] Therefore, IR spectra further affirm that TC was successfully loaded onto GO. The IR spectra of PDDA and AgNPs assembled GO was shown in Fig. 4**b**. For the free PDDA spectra, the peaks at the 1474 at 1640 cm^{-1} were attributed to the deformation vibration of C = C.[58] For the PDDA modified GO, the peak at 1731 cm^{-1} was decreased and shifted to 1724 cm^{-1}. The bands at 1635 and 1466 cm^{-1} correspond to the PDDA, indicating the presence of PDDA on the surface of GO.[59,60] After AgNPs assembled, the bands at 1645, 1527 and 1044 cm^{-1} were appear, corresponding to the C = O, C = C, and C-O stretching vibration of the biological corona group on the surface of green AgNPs.[39,61,62] The FTIR spectra of AgNPs is shown in the supplementary materials (**Figure S6**).

3.2. *Antimicrobial activity of the PDA/GO/TC and PDA/GO/Ag coatings*

The antimicrobial activity of the coatings was assessed using disc diffusion method (Kirby Bauer method).[63,64] Parallel experiments were conducted with the PDA, PDA/GO, PDA/GO/TC, and PDA/GO/Ag coatings, respectively. Coatings are named PDA/GO/TC_1 and PDA/GO/TC_2 meaning that the assembled concentration of TC is 1 and 2 mg/mL, respectively. The coating is named PDA/GO/Ag_{108} meaning that the

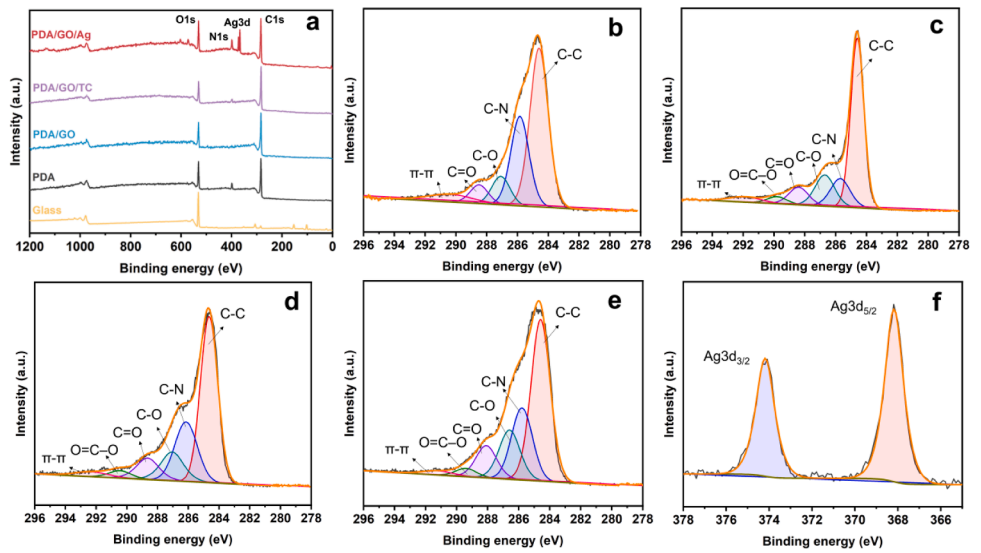

Fig. 3. Full scan XPS spectra of bare glass, PDA, PDA/GO, PDA/GO/TC and PDA/GO/Ag (a); high-resolution C1s spectrum of PDA (b), PDA/GO (c), PDA/GO/TC (d) and PDA/GO/Ag (e); high-resolution Ag3d spectrum of PDA/GO/Ag (f).

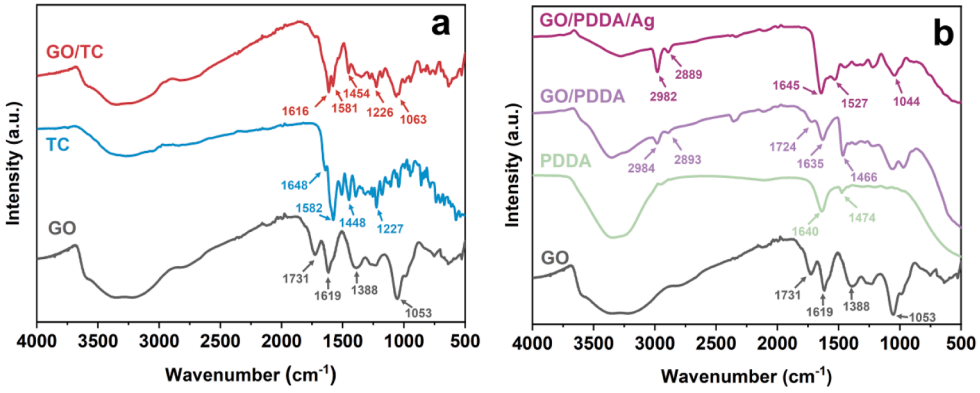

Fig. 4. (a) FTIR spectra of GO, TC and GO/TC; (b) FTIR spectra of GO, PDDA, GO/PDDA and GO/PDDA/Ag.

assembled concentration of AgNPs is 108 μg/mL. The antibacterial activity can be assessed by the zone of inhibition (Fig. 5**a, b**). Zones of inhibition appeared around the PDA/GO/TC and PDA/GO/Ag coatings on the agar plates during the first 24 h, indicating that bacteria around these coatings were inhibited or eliminated. However, no zone of inhibition was exhibited around the PDA and PDA/GO coatings on the agar plates, indicating that PDA and GO were not effective against *S. aureus* and *E. coli* growth in the present study. The results suggest that the antibacterial activity of the PDA/GO/TC and PDA/GO/Ag coatings came from TC and AgNPs loaded on GO. When TC was directly loaded on the glass without PDA/GO coating, it was found that TC could not be loaded on the glass surface, and the glass had no antibacterial effect, which further confirmed the effectiveness of the layer-by-layer assembly coating. Moreover, the statistical study of the disk diffusion was explored (Fig. 5**c, d**). From 24 to 96 h, the diameters of zone of inhibition remained unchanged over time, indicating that the PDA/GO/TC and PDA/GO/Ag coatings could maintain high antibacterial activity against *E. coli* and *S. aureus* bacteria.

3.3. Biofilm inhibition by PDA/GO/TC and PDA/GO/Ag coatings

Biofilms are considered a key factor in medical devices and biomedical implants.[65] Advances in the design and development of anti-biofilm coatings provide opportunities to produce biofilm resistant devices.[66] The prepared PDA/GO/TC and PDA/GO/Ag coatings are expected to prevent biofilm formation for protecting the surfaces of biomedical devices. To investigate the anti-biofilm activity, two pathogens, gram-negative bacteria *E. coli* and gram-positive bacteria *S. aureus* were incubated with PDA/GO/TC coatings. Bacterial biofilms were grown on TC loaded coating PDA/GO/TC for 24 h. Viable bacterial were counted (Fig. 6**a, b**). Compared with the control sample, the PDA and PDA/GO coatings, scarcely showed antibiofilm effects. These results are consistent with previous reports.[15,18] The parallel oriented GO coating does not produce sharp edges for puncturing bacterial cells. This surface-parallel coating has been reported to have adsorption capacity, and in fact facilitates bacterial cell adhesion and promotes biofilm growth.[6768] In addition, most of the bactericidal effects of GO are reflected in the planktonic environment. Bacterial cells in biofilms are harder to fight than planktonic bacteria and the anti-biofilm effect may be also related to the cell incubation time.[6970] Here, the effects of PDA/GO were extremely limited during the 24-hour process of bacterial attachment, colonization and biofilm dispersion on the coating. However, the PDA/GO/TC coatings inhibited the formation of *S. aureus* and *E. coli* biofilms by a factor of more than 1000 (3 $\log_{10}$ units). The results indicate that TC on the coated surface contributes to the inhibition of biofilm. Notably, when TC was directly assembled on the surface of PDA without the help of GO, the coatings did not exhibit any inhibitory effect on biofilms (**Figure S7**). The loading of TC on the PDA coating surface

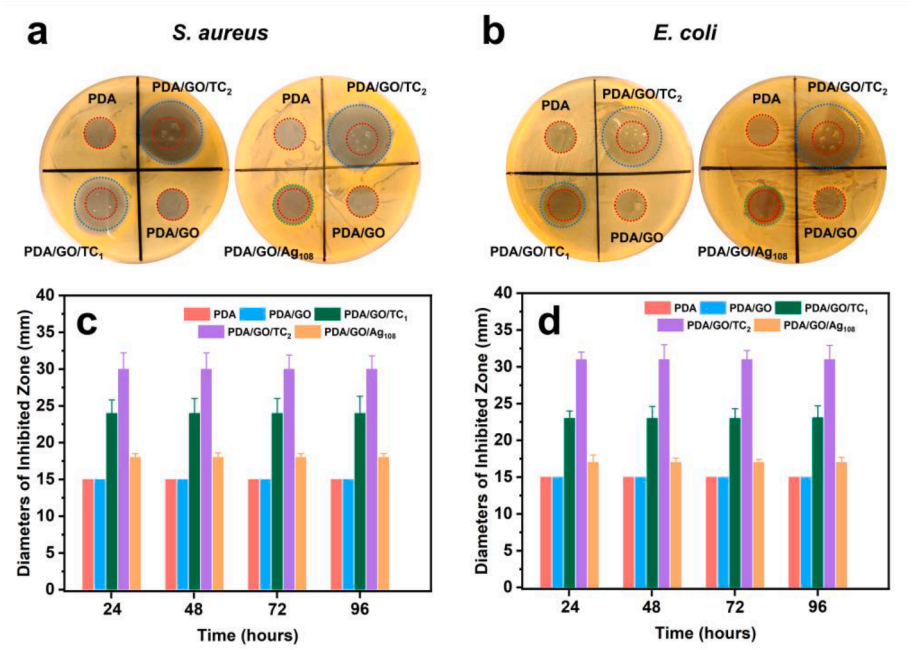

Fig. 5. The zone of inhibition of coatings in the Kirby-Bauer diffusion test. PDA, PDA/GO, PDA/GO/TC and PDA/GO/Ag coatings are placed on a lawn of S. aureus (a) and E. coli (b) on an agar medium plate. The columns demonstrate the zone of inhibition diameters for different coatings in S. aureus (c) and E. coli (d).

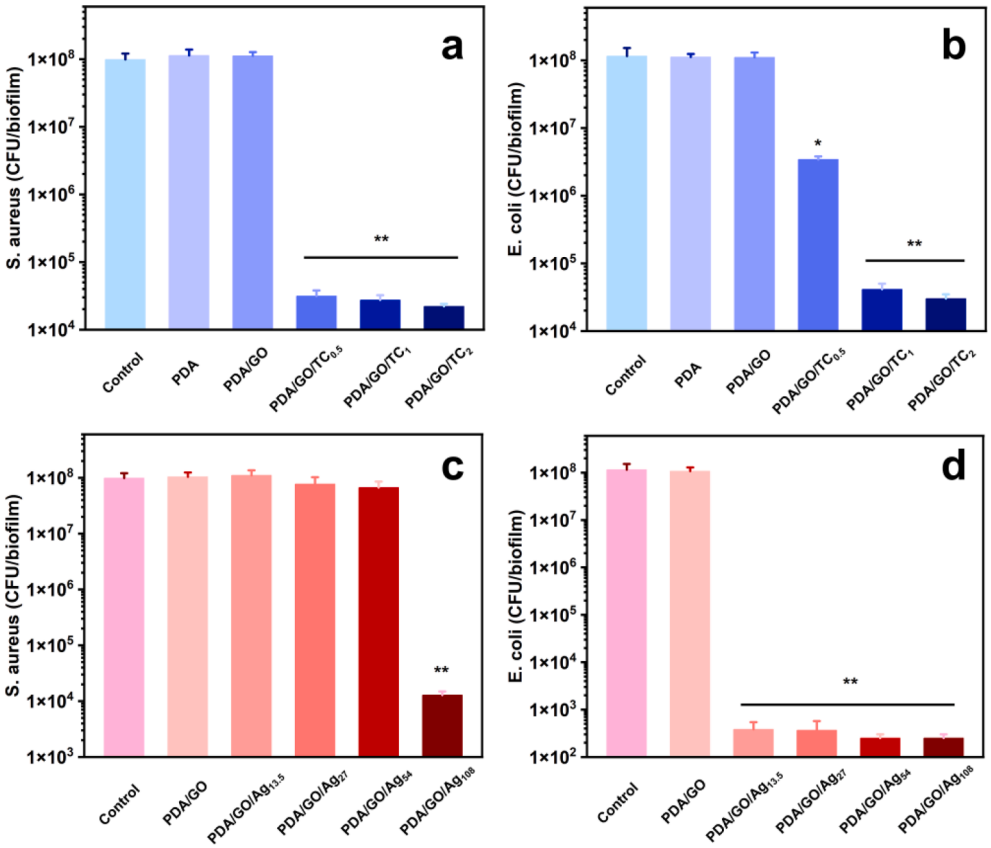

Fig. 6. CFU counts of PDA/GO/TC against (a) S. aureus and (b) E. coli and PDA/GO/Ag coatings against (c) S. aureus and (d) E. coli after 24 h biofilm growth. *P < 0.05, **P < 0.005.

was not observed as quantified by UV–vis spectroscopy. In addition to that, no changes in the chemical state of the elements in XPS spectra before and after loading TC suggests that the loading of TC on the PDA modified surface is extremely limited. The high loading capacity of GO determines the effective adsorption and release of the drug. In the same way, *E. coli* and *S. aureus* were incubated with PDA/GO/Ag coatings. Bacterial biofilms were grown on AgNPs assembled coating PDA/GO/Ag for 24 h (Fig. 6**c, d**). It can be seen that PDA/GO/Ag coatings inhibited

the formation of *E. coli* biofilms by a factor of more than 100000 (5 $\log_{10}$ units) at all AgNPs adsorption concentrations (13.5, 27, 54, and 108 μg/mL). It is worth noting that the inhibitory effect of AgNPs coating on *E. coli* biofilm was stronger than that of TC coating. However, the PDA/GO/Ag coatings inhibited the formation of *S. aureus* biofilms only at high adsorption concentrations (108 μg/mL). It was found that concentration-independent inhibition of biofilm formation was observed against *E. coli*. It was observed that the PDA/GO/Ag coating had a weaker biofilm inhibition efficiency against *S. aureus*. Our previous study showed that the green AgNPs in this work completely inhibited the bacterial growth of the Gram-negative bacterium *Pseudomonas aeruginosa* at 1 μg/mL.[39] While the minimum inhibitory concentrations of AgNPs against *E.coli* and *S. aureus* were 6.25 μg/mL and 100 μg/ml, respectively. Thus, it was obvious that PDA/GO/Ag coatings were not effective against *S. aureus*.

Several factors affect the antimicrobial activity of green AgNPs, such as size, shape, surface charge, and most importantly, the corona surrounding the AgNPs.[71] The corona is formed while synthesizing the AgNPs. During antimicrobial treatment, the thickness of these corona layers increases due to the addition of proteins or components released from pathogens, which facilitates the internalization of AgNPs. The corona layer interacts with the pathogen's membrane and helps the AgNPs to function.[39] The main difference in antimicrobial efficacy against these two bacteria could be attributed to differences in the surface of the bacteria.[72,73] Gram-positive bacteria have a thick coating (20–80 nm) composed of negatively charged peptidoglycan, which may hinder the penetration of AgNPs and weaken the activity of silver ions, resulting in a weaker overall antibacterial effect. In contrast, the thinner cell envelope (8–12 nm) of Gram-negative bacteria renders bacterial cells more susceptible to the AgNPs treatment.[74] Another contributing factor may be the total charge on the bacterial cell surface. The surface of Gram-negative bacteria generally has a lower isoelectric point (pH 2) compared to the surface of Gram-positive bacteria (pH 3–4). Gram-positive bacteria may have a better ability to neutralize the charged functional groups in the coating of AgNPs, thereby reducing their ability to interact with target cells.[75] Although the bacterial growth inhibitory effect of our AgNPs on Gram-positive bacteria was lower compared to Gram-negative bacteria, they still had an inhibitory effect on biofilm formation at certain concentration. The release and accumulation of silver ions can penetrate bacterial cells by binding to thiol groups present in enzymes, which may inhibit the growth of biofilms by increasing reactive oxygen species, altering gene expression and metabolic activities, or inhibiting quorum sensing within biofilms.[76] In addition, the antibacterial effect of green-synthesized AgNPs and chemically synthesized AgNPs may be different due to the presence of corona layer. The next step of this work will consist in performing the loading and release of AgNPs on PDA/GO/Ag coatings and the study of the mechanisms underlying the difference in inhibition of Gram-positive and Gram-negative bacteria.

The reduction in CFU counts of biofilms could result from the inhibitory effect of coatings on bacterial adhesion or result from the bactericidal activity of released drugs from the coating. The ability of the coatings to resist biofilm formation was also determined by live/dead fluorescence images (Fig. 7). No dead cells and no loss of bacterial adhesion was found on the coatings without TC and AgNPs. However, dead cells (stained red) were observed on the PDA/GO/TC and PDA/GO/Ag coatings and the overall number of living cells is lower. This shows that these coatings not only kill bacteria, but also effectively prevent the adhesion of bacteria on the surface.

Furthermore, to visualize the morphological changes of the biofilm cells on the antimicrobial coating, the biofilms were examined by SEM imaging (Fig. 8). Similar trend of antibiofilm efficiency was observed from SEM analysis compared to live/dead staining. The control coating and the PDA/GO coating surface had a dense biofilm structure with some exopolysaccharide matrix. The biofilms on the PDA/GO/TC and PDA/GO/Ag coatings showed a significant degree of morphological alteration. Few bacterial cells were detected, and no complete biofilm was formed. Judging from the fact that the PDA/GO coating did not significantly inhibit the bacterial biofilm, the anti-biofilm properties were mainly due to the contribution of TC and AgNPs. TC form a reversible combination with the 16S rRNA of the 30S subunit of the ribosome of the bacterial cell to inhibit protein synthesis and play an

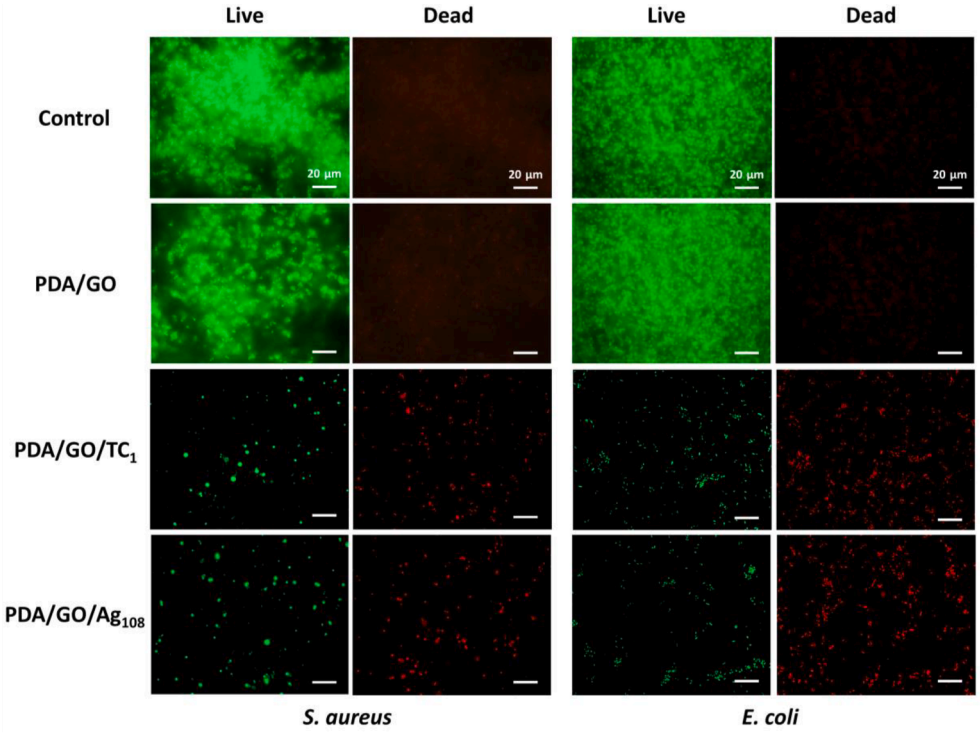

Fig. 7. Live/dead fluorescent staining of S. aureus and E. coli. Biofilm on the coatings. Green indicates live bacteria and red indicates dead bacteria.

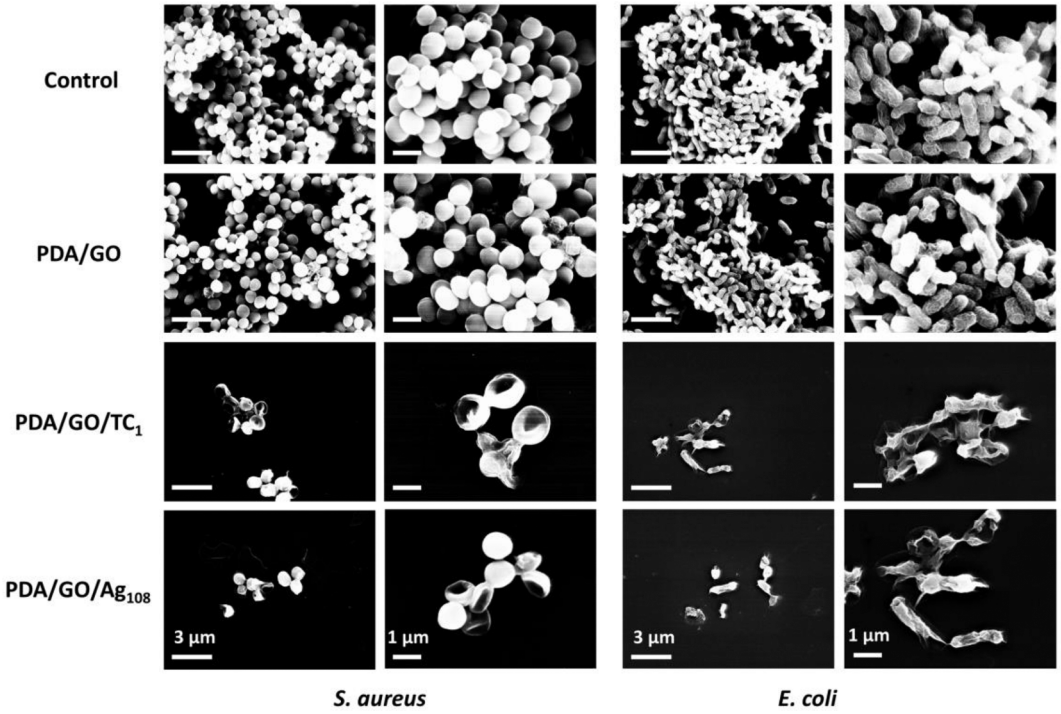

Fig. 8. Representative SEM images of S. aureus and E. coli biofilms grown on the PDA/GO/TC and PDA/GO/Ag coatings.

antibacterial effect. Here, the released TC from PDA/GO/TC coatings could inhibit bacterial protein synthesis efficiently.[77] The green AgNPs used in this study inhibited biofilm formation, possibly due to the bacterial membranes contacting and attaching to the nanoparticles on the coating surface and causing cell lysis. It is also possible that endocytosis or engulfment of AgNPs by cells leads to various effects, such as ROS production, DNA damage, inhibition of proteins and ribosomes functions.[39].

To examine the biocompatibility of the antibacterial coatings, the Huh7 human hepatoma cell were cultured with bare glass, PDA/GO, PDA/GO/TC_1, PDA/GO/Ag_{108} coatings samples. The result of the alamarBlue assay is shown in **Figure S8**. Compared with the bare glass samples, no significant difference in cell viability is observed in the PDA/GO sample. Slightly decreased cell viability is found on the PDA/GO/TC_1 and PDA/GO/Ag_{108} samples compared with the bare glass samples, but still higher than the medium control. These results indicate that the antibacterial coatings prepared in this study are biocompatible.

Whether antibiofilm effects of the PDA/GO/TC coating would persist for longer time periods were tested. Viable counts were recorded for 3 days. The culture medium was replaced every 24 h. The biofilms after each day were collected, serially diluted and homogenized and plated on agar plates to count the colonies. The results of antibacterial persistence were included in **Figure S9**. No obvious increase of viability of biofilms was seen in the CFU results of 3 days. The antibiofilm activities remained strong with a 1000-fold (3 $\log_{10}$ units) reduction in viable cell count. It comes from the inhibitory effects during the release of TC, which can effectively prevent the growth of biofilm for a long time. The cumulative TC release amount from the PDA/GO/TC_1 coating were determined. The total amount of TC loaded onto the PDA/GO coating was around 90 μg. The cumulative release percentage of TC reached the maximum after around three days that nearly 89 % of TC was released from the coating (**Figure S10**). The burst release of TC from the PDA/GO/TC coating was observed on the first day and the amount of released TC became gradually lower on the next several days, indicating the near-complete release of the TC in around three days. When the drug without a carrier is exposed to a liquid medium, the release rate is unavoidably fast.[78,79] The drug release from the coating is due to gradual drug diffusion through the coating matrix.[80,81] Although the prolonged release is preferred for drug delivery for the treatment,[82] the coating in this work acts as an antibiofilm coating due to the burst release effect which can ensure high drug concentration in a localized area in a short time, thus preventing the bacterial colonization to biomedical devices.

The versatility, ease of preparation, and durability of coatings are important for application to biomedical devices. Various techniques have been developed to fabricate coatings including electrochemical deposition, sol–gel techniques, chemical vapor deposition (CVD) and spraying.[83] These technologies can improve tissue integration, drug delivery and promote wound healing. Substrate selectivity of the surface coating, preparation conditions, process cost, reproducibility and stability are all factors to be considered to develop ideal biomedical coatings. The PDA coating requires only facile and versatile processing conditions and exhibits unique stability, mechanical properties and strong adhesion to a variety of organic and inorganic matrix materials.[84,85] The PDA is very beneficial to the subsequent material assembly. There is reason to suggest that our coatings have the potential to be applied to a variety of medical device materials, such as coatings for dental, orthopedic, and cardiovascular implants. Although, broad-spectrum antibiotics and green Ag nanoparticles were used in this study, more anti-biofilm inhibitors such as antimicrobial peptides (AMPs) and enzymes are worth trying on this coating.[86] Grafting coatings to the surface of medical materials such as medical catheters are the next focus, and the duration and stability of coatings *in vivo* are also worth investigating.[87].

4. Conclusions

Summarily, in this work, anti-biofilm coatings of PDA/GO/TC and PDA/GO/Ag were developed by layer-by-layer assembly. This is the first time to load TC and AgNPs as antibacterial agents onto PDA/GO multifunctional coatings. These coatings benefit from the adhesion ability of PDA and the high loading capacity of GO. The successful loading and release of antibiotic and green synthesized AgNPs on the surface of GO ensure that the coating has excellent anti-biofilm properties. This anti-biofilm coatings have several advantages. PDA can be

adsorbed on the surface of almost all substances to form a film, which constitutes the basis for the versatility of this antibacterial coating. GO has a super-strong surface loading capacity, which provides diversity for the loading of various functional antibiotics and other agents such as peptide or AgNPs. Green-soft methods and highly biocompatible materials are used in the preparation of the coating, which could be a potential approach to prevent bacterial adhesion and infection of implantable biomedical devices *in vivo*.

Funding

This work was supported by the Novo Nordisk Foundation (NNF10CC1016517), Nord Forsk (Project No. 105121), Lundbeckfonden (R303-2018–3499), Novo Nordisk Foundation (NNF20OC0064547), Vetenskapsrådet (2020–04096).

CRediT authorship contribution statement

Jian Zhang: Conceptualization, Methodology, Data curation, Formal analysis, Investigation, Writing – original draft, Writing – review & editing. **Priyanka Singh:** Methodology, Data curation, Investigation, Writing – review & editing. **Zhejian Cao:** Methodology, Data curation, Investigation, Writing – review & editing. **Shadi Rahimi:** Methodology, Data curation, Investigation, Writing – review & editing. **Santosh Pandit:** Conceptualization, Data curation, Formal analysis, Investigation, Methodology, Supervision, Writing – review & editing. **Ivan Mijakovic:** Conceptualization, Data curation, Formal analysis, Funding acquisition, Investigation, Methodology, Project administration, Supervision, Validation, Writing – review & editing.

Declaration of Competing Interest

The authors declare that they have no known competing financial interests or personal relationships that could have appeared to influence the work reported in this paper.

Data availability

Data will be made available on request.

Appendix A. Supplementary material

Supplementary data to this article can be found online at https://doi.org/10.1016/j.apsusc.2023.157221.

References

[1] S.L. Percival, L. Suleman, C. Vuotto, G. Donelli, Healthcare-associated infections, medical devices and biofilms: risk, tolerance and control, J. Med. Microbiol. 64 (2015) 323–334, https://doi.org/10.1099/jmm.0.000032.
[2] P.S. Stewart, J.W. Costerton, Antibiotic resistance of bacteria in biofilms, The Lancet 358 (2001) 135–138, https://doi.org/10.1016/S0140-6736(01)05321-1.
[3] A. Singh, A. Amod, P. Pandey, P. Bose, M.S. Pingali, S. Shivalkar, P.K. Varadwaj, A. K. Sahoo, S.K. Samanta, Bacterial biofilm infections, their resistance to antibiotics therapy and current treatment strategies, Biomed. Mater. 17 (2022), 022003, https://doi.org/10.1088/1748-605X/ac50f6.
[4] I. Francolini, G. Donelli, Prevention and control of biofilm-based medical-device-related infections, FEMS Immunol. Med. Microbiol. 59 (2010) 227–238, https://doi.org/10.1111/j.1574-695X.2010.00665.x.
[5] P. Makvandi, C. Wang, E.N. Zare, A. Borzacchiello, L. Niu, F.R. Tay, Metal-based nanomaterials in biomedical applications: antimicrobial activity and cytotoxicity aspects, Adv. Funct. Mater. 30 (2020) 1910021, https://doi.org/10.1002/adfm.201910021.
[6] Y. Jiang, M. Geng, L. Bai, Targeting biofilms therapy: current research strategies and development hurdles, Microorganisms 8 (2020) 1222, https://doi.org/10.3390/microorganisms8081222.
[7] J. Haider, A. Shahzadi, M.U. Akbar, I. Hafeez, I. Shahzadi, A. Khalid, A. Ashfaq, S. O.A. Ahmad, S. Dilpazir, M. Imran, M. Ikram, G. Ali, M. Khan, Q. Khan, M. Maqbool, A review of synthesis, fabrication, and emerging biomedical applications of metal-organic frameworks, Biomater. Adv. (2022), 213049, https://doi.org/10.1016/j.bioadv.2022.213049.
[8] Y. Liu, L. Shi, L. Su, H.C. van der Mei, P.C. Jutte, Y. Ren, H.J. Busscher, Nanotechnology-based antimicrobials and delivery systems for biofilm-infection control, Chem. Soc. Rev. 48 (2019) 428–446, https://doi.org/10.1039/C7CS00807D.
[9] S. Qayyum, A.U. Khan, Nanoparticles vs. biofilms: a battle against another paradigm of antibiotic resistance, MedChemComm 7 (2016) 1479–1798, https://doi.org/10.1039/C6MD00124F.
[10] W. Wei, J. Li, Z. Liu, Y. Deng, D. Chen, P. Gu, G. Wang, X. Fan, Distinct antibacterial activity of a vertically aligned graphene coating against Gram-positive and Gram-negative bacteria, J. Mater. Chem. B 8 (2020) 6069–6079, https://doi.org/10.1039/D0TB00417K.
[11] K.S. Novoselov, V.I. Fal'ko, L. Colombo, P.R. Gellert, M.G. Schwab, K. Kim, A roadmap for graphene, Nature 490 (2012) 192–200, https://doi.org/10.1038/nature11458.
[12] D. Dai, D. Zhou, H. Xie, J. Wang, C. Zhang, The design, construction and application of graphene family composite nanocoating on dental metal surface, Biomater. Adv. (2022), 213087, https://doi.org/10.1016/j.bioadv.2022.213087.
[13] X. Sun, X. Yu, W. Li, M. Chen, D. Liu, Mechanical properties, degradation behavior and cytocompatibility of biodegradable 3vol%X (X = MgO, ZnO and CuO)/Zn matrix composites with excellent dispersion property fabricated by graphene oxide-assisted hetero-aggregation, Biomater. Adv. (2022), 112722, https://doi.org/10.1016/j.msec.2022.112722.
[14] Y. Tu, M. Lv, P. Xiu, T. Huynh, M. Zhang, M. Castelli, Z. Liu, Q. Huang, C. Fan, H. Fang, R. Zhou, Destructive extraction of phospholipids from Escherichia coli membranes by graphene nanosheets, Nat. Nanotechnol. 8 (2013) 594–601, https://doi.org/10.1038/nnano.2013.125.
[15] S. Pandit, Z. Cao, V.R.S.S. Mokkapati, E. Celauro, A. Yurgens, M. Lovmar, F. Westerlund, J. Sun, I. Mijakovic, Vertically aligned graphene coating is bactericidal and prevents the formation of bacterial biofilms, Adv. Mater. Interfaces 5 (2018) 1701331, https://doi.org/10.1002/admi.201701331.
[16] Y. Zhu, S. Murali, W. Cai, X. Li, J.W. Suk, J.R. Potts, R.S. Ruoff, Graphene and graphene oxide: synthesis, properties, and applications, Adv. Mater. 22 (2010) 3906–3924, https://doi.org/10.1002/adma.201001068.
[17] Y. Esmaeili, H.S. Ghaheh, F. Ghasemi, L. Shariati, M. Rafienia, E. Bidram, A. Zarrabi, Graphene oxide quantum dot-chitosan nanotheranostic platform as a pH-responsive carrier for improving curcumin uptake internalization: In vitro & in silico study, Biomaterials Advances (2022) 213017, https://doi.org/10.1016/j.bioadv.2022.213017.
[18] X. Lu, X. Feng, J.R. Werber, C. Chu, I. Zucker, J.-H. Kim, C.O. Osuji, M. Elimelech, Enhanced antibacterial activity through the controlled alignment of graphene oxide nanosheets, Proceedings of the national academy of sciences 114 (2017) 9793-9801, https://doi.org/10.1073/pnas.1710996114.
[19] S. Liu, M. Hu, T.H. Zeng, R. Wu, R. Jiang, J. Wei, L. Wang, J. Kong, Y. Chen, Lateral dimension-dependent antibacterial activity of graphene oxide sheets, Langmuir 28 (2012) 12364–12372, https://doi.org/10.1021/la3023908.
[20] S. Gurunathan, J.W. Han, A.A. Dayem, V. Eppakayala, J.-H. Kim, Oxidative stress-mediated antibacterial activity of graphene oxide and reduced graphene oxide in Pseudomonas aeruginosa, International journal of nanomedicine 7 (2012) 5901, https://doi.org/10.2147%2FIJN.S37397.
[21] L. Jiang, C. Su, S. Ye, J. Wu, Z. Zhu, Y. Wen, R. Zhang, W. Shao, Synergistic antibacterial effect of tetracycline hydrochloride loaded functionalized graphene oxide nanostructures, Nanotechnology 29 (2018), 505102, https://doi.org/10.1088/1361-6528/aae424.
[22] H.N. Abdelhamid, M.S. Khan, H.F. Wu, Graphene oxide as a nanocarrier for gramicidin (GOGD) for high antibacterial performance, RSC Adv. 4 (2014) 50035–50046, https://doi.org/10.1039/C4RA07250B.
[23] X. Hao, S. Chen, H. Zhu, L. Wang, Y. Zhang, Y. Yin, The synergy of graphene oxide and polydopamine assisted immobilization of lysozyme to improve antibacterial properties, ChemistrySelect 2 (2017) 2174–2182, https://doi.org/10.1002/slct.201601794.
[24] X. Pei, Z. Zhu, Z. Gan, J. Chen, X. Zhang, X. Cheng, Q. Wan, J. Wang, PEGylated nano-graphene oxide as a nanocarrier for delivering mixed anticancer drugs to improve anticancer activity, Sci. Rep. 10 (2020) 1–5, https://doi.org/10.1038/s41598-020-59624-w.
[25] H. Lee, S.M. Dellatore, W.M. Miller, P.B. Messersmith, Mussel-inspired surface chemistry for multifunctional coatings, Science 318 (2007) 426–430, https://doi.org/10.1126/science.1147241.
[26] G. Yeroslavsky, O. Girshevitz, J. Foster-Frey, D.M. Donovan, S. Rahimipour, Antibacterial and antibiofilm surfaces through polydopamine-assisted immobilization of lysostaphin as an antibacterial enzyme, Langmuir 31 (2015) 1064–1073, https://doi.org/10.1021/la503911m.
[27] H. Chen, L. Zhao, D. Chen, W. Hu, Stabilization of gold nanoparticles on glass surface with polydopamine thin film for reliable LSPR sensing, J. Colloid Interface Sci. 460 (2015) 258–263, https://doi.org/10.1016/j.jcis.2015.08.075.
[28] H.M. Hegab, A. ElMekawy, T.G. Barclay, A. Michelmore, L. Zou, C.P. Saint, M. Ginic-Markovic, Effective in-situ chemical surface modification of forward osmosis membranes with polydopamine-induced graphene oxide for biofouling mitigation, Desalination 385 (2016) 126–137, https://doi.org/10.1016/j.desal.2016.02.021.
[29] C. Lin, L. Chung, G. Lin, M. Chang, C. Lee, N.-H. Tai, Enhancing the efficiency of a forward osmosis membrane with a polydopamine/graphene oxide layer prepared via the modified molecular layer-by-layer method, ACS Omega 5 (2020) 18738–18745, https://doi.org/10.1021/acsomega.0c01752.
[30] C. Fang, Y. Deng, Y. Xie, J. Su, G. Chen, Improving the electrochemical performance of Si nanoparticle anode material by synergistic strategies of

polydopamine and graphene oxide coatings, J. Phys. Chem. C 119 (2015) 1720–1728, https://doi.org/10.1021/jp511179s.
[31] B. Le Ouay, F. Stellacci, Antibacterial activity of silver nanoparticles: a surface science insight, Nano Today 10 (2015) 339–354, https://doi.org/10.1016/j.nantod.2015.04.002.
[32] H. Barabadi, F. Mojab, H. Vahidi, B. Marashi, N. Talank, O. Hosseini, M. Saravanan, Green synthesis, characterization, antibacterial and biofilm inhibitory activity of silver nanoparticles compared to commercial silver nanoparticles, Inorg. Chem. Commun. 129 (2021), 108647, https://doi.org/10.1016/j.inoche.2021.108647.
[33] P. Singh, I. Mijakovic, Green synthesis and antibacterial applications of gold and silver nanoparticles from Ligustrum vulgare berries, Sci. Rep. 12 (2022) 1–12, https://doi.org/10.1038/s41598-022-11811-7.
[34] P. Singh, S. Pandit, J. Garnæs, S. Tunjic, V. RSS Mokkapati, A. Sultan, A. Thygesen, A. Mackevica, R.V. Mateiu, A.E. Daugaard, A. Baun, I. Mijakovic, Green synthesis of gold and silver nanoparticles from Cannabis sativa (industrial hemp) and their capacity for biofilm inhibition, International journal of nanomedicine 13 (2018) 3571, https://doi.org/10.2147/IJN.S157958.
[35] J. Jang, J.M. Lee, S.B. Oh, Y. Choi, H.S. Jung, J. Choi, Development of antibiofilm nanocomposites: Ag/Cu c nanoparticles synthesized on the surface of graphene oxide nanosheets, ACS Appl. Mater. Interfaces 12 (2020) 35826–35834, https://doi.org/10.1021/acsami.0c06054.
[36] Z. Zhang, J. Zhang, B. Zhang, J. Tang, Mussel-inspired functionalization of graphene for synthesizing Ag-polydopamine-graphene nanosheets as antibacterial materials, Nanoscale 5 (2013) 118–123, https://doi.org/10.1039/C2NR32092D.
[37] H. Zhou, Y. Liu, W. Chi, C. Yu, Y. Yu, Preparation and antibacterial properties of Ag@polydopamine/graphene oxide sheet nanocomposite, Appl. Surf. Sci. 282 (2013) 181–185, https://doi.org/10.1016/j.apsusc.2013.05.099.
[38] Y. Zhang, S. Chen, J. An, H. Fu, X. Wu, C. Pang, H. Gao, Construction of an antibacterial membrane based on dopamine and polyethylenimine cross-linked graphene oxide, ACS Biomater. Sci. Eng. 5 (2019) 2732–2739, https://doi.org/10.1021/acsbiomaterials.9b00061.
[39] P. Singh, I. Mijakovic, Antibacterial effect of silver nanoparticles is stronger if the production host and the targeted pathogen are closely related, Biomedicines 10 (2022) 628, https://doi.org/10.3390/biomedicines10030628.
[40] N. Sarviya, U. Mahanta, A. Dart, J. Giri, A.S. Deshpande, M. Khandelwal, M. Bhave, P. Kingshott, Biocompatible and antimicrobial multilayer fibrous polymeric wound dressing with optimally embedded silver nanoparticles, Appl. Surf. Sci. 612 (2023), 155799, https://doi.org/10.1016/j.apsusc.2022.155799.
[41] A. Rahman, S.C. Kang, In vitro control of food-borne and food spoilage bacteria by essential oil and ethanol extracts of Lonicera japonica Thunb, Food Chem. 116 (2009) 670–675, https://doi.org/10.1016/j.foodchem.2009.03.014.
[42] Di. Bogdan, I.-G. Grosu, C .Filip, How thick, uniform and smooth are the polydopamine coating layers obtained under different oxidation conditions? An in-depth AFM study. Applied Surface Science (2022) 153680, https://doi.org/10.1016/j.apsusc.2022.153680.
[43] S.R.V. Castrillón, F. Perreault, A.F.D. Faria, M. Elimelech, Interaction of graphene oxide with bacterial cell membranes: insights from force spectroscopy, Environ. Sci. Technol. Lett. 2 (2015) 112–117, https://doi.org/10.1021/acs.estlett.5b00066.
[44] W. Ren, Y. Fang, E. Wang, A binary functional substrate for enrichment and ultrasensitive SERS spectroscopic detection of folic acid using graphene oxide/Ag nanoparticle hybrids, Acs Nano 5 (2011) 6425–6433, https://doi.org/10.1021/nn201606r.
[45] A.C. Ferrari, D.M. Basko, Raman spectroscopy as a versatile tool for studying the properties of graphene, Nat. Nanotechnol. 8 (2013) 235–246, https://doi.org/10.1038/nnano.2013.46.
[46] A.K. Yadav, P. Singh, A review of the structures of oxide glasses by Raman spectroscopy, RSC Adv. 5 (2015) 67583–67609, https://doi.org/10.1039/C5RA13043C.
[47] A.C. Ferrari, Raman spectroscopy of graphene and graphite: disorder, electron–phonon coupling, doping and nonadiabatic effects, Solid State Commun. 143 (2007) 47–57, https://doi.org/10.1016/j.ssc.2007.03.052.
[48] C. Silva, F. Simon, P. Friedel, P. Pötschke, C. Zimmerer, Elucidating the chemistry behind the reduction of graphene oxide using a green approach with polydopamine, Nanomaterials 9 (2019) 902, https://doi.org/10.3390/nano9060902.
[49] R. Beams, L.G. Cançado, L. Novotny, Raman characterization of defects and dopants in graphene, J. Phys. Condens. Matter 27 (2015), 083002, https://doi.org/10.1088/0953-8984/27/8/083002.
[50] J. Serra, P. González, S. Liste, C. Serra, S. Chiussi, B. León, M. Pérez-Amor, H. O. Ylänen, M. Hupa, FTIR and XPS studies of bioactive silica based glasses, J. Non Cryst. Solids 332 (2003) 20–27, https://doi.org/10.1016/j.jnoncrysol.2003.09.013.
[51] Y. Feng, X. Ma, L. Chang, S. Zhu, S. Guan, Characterization and cytocompatibility of polydopamine on MAO-HA coating supported on Mg-Zn-Ca alloy, Surf. Interface Anal. 49 (2017) 1115–1123, https://doi.org/10.1002/sia.6286.
[52] R.A. Zangmeister, T.A. Morris, M.J. Tarlov, Characterization of polydopamine thin films deposited at short times by autoxidation of dopamine, Langmuir 29 (2013) 8619–8628, https://doi.org/10.1021/la400587j.
[53] Y. Lv, Z. Niu, Y. Chen, Y. Hu, Bacterial effects and interfacial inactivation mechanism of nZVI/Pd on Pseudomonas putida strain, Water Res. 115 (2017) 297–308, https://doi.org/10.1016/j.watres.2017.03.012.
[54] P. Anbu, S.C.B. Gopinath, H.S. Yun, C.-G. Lee, Temperature-dependent green biosynthesis and characterization of silver nanoparticles using balloon flower plants and their antibacterial potential, J. Mol. Struct. 1177 (2019) 302–309, https://doi.org/10.1016/j.molstruc.2018.09.075.
[55] A.K. Potbhare, P.B. Chouke, A. Mondal, R.U. Thakare, S. Mondal, R.G. Chaudhary, A.R. Rai, Rhizoctonia solani assisted biosynthesis of silver nanoparticles for antibacterial assay, Mater. Today:. Proc. 29 (2020) 939–945, https://doi.org/10.1016/j.matpr.2020.05.419.
[56] Rattana, S. Chaiyakun, N. Witit-anun, N. Nuntawong, P. Chindaudom, S. Oaew, C. Kedkeaw, P. Limsuwan, Preparation and characterization of graphene oxide nanosheets, Procedia Engineering 32 (2012) 759-764, https://doi.org/10.1016/j.proeng.2012.02.009.
[57] E.E. Ghadim, F. Manouchehri, G. Soleimani, H. Hosseini, S. Kimiagar, S. Nafisi, Adsorption properties of tetracycline onto graphene oxide: equilibrium, kinetic and thermodynamic studies, PLoS One 8 (2013) e79254.
[58] D. Yang, J.-F. Rochette, E. Sacher, Spectroscopic evidence for π−π interaction between poly (diallyl dimethylammonium) chloride and multiwalled carbon nanotubes, J. Phys. Chem. B 109 (2005) 4481–4484, https://doi.org/10.1021/jp044511+.
[59] K. Liu, J. Zhang, G. Yang, C. Wang, J. Zhu, Direct electrochemistry and electrocatalysis of hemoglobin based on poly (diallyldimethylammonium chloride) functionalized graphene sheets/room temperature ionic liquid composite film, Electrochem. Commun. 12 (2010) 402–405, https://doi.org/10.1016/j.elecom.2010.01.004.
[60] M. Zhang, J. Xie, Q. Sun, Z. Yan, M. Chen, J. Jing, Enhanced electrocatalytic activity of high Pt-loadings on surface functionalized graphene nanosheets for methanol oxidation, Int. J. Hydrogen Energy 38 (2013) 16402–16409, https://doi.org/10.1016/j.ijhydene.2013.09.108.
[61] J. Jayabalan, G. Mani, N. Krishnan, J. Pernabas, J.M. Devadoss, H.T. Jang, Green biogenic synthesis of zinc oxide nanoparticles using Pseudomonas putida culture and its In vitro antibacterial and anti-biofilm activity, Biocatal. Agric. Biotechnol. 21 (2019), 101327, https://doi.org/10.1016/j.bcab.2019.101327.
[62] R.A. Hamouda, M.H. Hussein, R.A. Abo-Elmagd, S.S. Bawazir, Synthesis and biological characterization of silver nanoparticles derived from the cyanobacterium Oscillatoria limnetica, Sci. Rep. 9 (2019) 1–7, https://doi.org/10.1038/s41598-019-49444-y.
[63] Z. Li, H. Tang, W. Yuan, W. Song, Y. Niu, L. Yan, M. Yu, M. Dai, S. Feng, M. Wang, Ag nanoparticle–ZnO nanowire hybrid nanostructures as enhanced and robust antimicrobial textiles via a green chemical approach, Nanotechnology 25 (2014), 145702, https://doi.org/10.1088/0957-4484/25/14/145702.
[64] J. Song, Q. Chen, Y. Zhang, M. Diba, E. Kolwijck, J. Shao, J.A. Jansen, F. Yang, A. R. Boccaccini, S.C.G. Leeuwenburgh, Electrophoretic deposition of chitosan coatings modified with gelatin nanospheres to tune the release of antibiotics, ACS Appl. Mater. Interfaces 8 (2016) 13785–13792, https://doi.org/10.1021/acsami.6b03454.
[65] D. Lebeaux, J.-M. Ghigo, C. Beloin, Biofilm-related infections: bridging the gap between clinical management and fundamental aspects of recalcitrance toward antibiotics, Microbiol. Mol. Biol. Rev. 78 (2014) 510–543, https://doi.org/10.1128/MMBR.00013-14.
[66] S. Bohara, J. Suthakorn, Surface coating of orthopedic implant to enhance the osseointegration and reduction of bacterial colonization: a review, Biomater. Res. 26 (2022) 1–17, https://doi.org/10.1186/s40824-022-00269-3.
[67] B. Ramalingam, T. Parandhaman, P. Choudhary, S.K. Das, Biomaterial functionalized graphene-magnetite nanocomposite: a novel approach for simultaneous removal of anionic dyes and heavy-metal ions, ACS Sustain. Chem. Eng. 6 (2018) 6328–6341, https://doi.org/10.1021/acssuschemeng.8b00139.
[68] T. Parandhaman, S.K. Das, Facile synthesis, biofilm disruption properties and biocompatibility study of a poly-cationic peptide functionalized graphene–silver nanocomposite, Biomater. Sci. 6 (2018) 3356–3372, https://doi.org/10.1039/C8BM01003J.
[69] S. Liu, T.H. Zeng, M. Hofmann, E. Burcombe, J. Wei, R. Jiang, J. Kong, Y. Chen, Antibacterial activity of graphite, graphite oxide, graphene oxide, and reduced graphene oxide: membrane and oxidative stress, ACS Nano 5 (2011) 6971–6980, https://doi.org/10.1021/nn202451x.
[70] J.D. Mangadlao, C.M. Santos, M.J.L. Felipe, A.C.C. de Leon, D.F. Rodrigues, R. C. Advincula, On the antibacterial mechanism of graphene oxide (GO) Langmuir-Blodgett films, Chem. Commun. 51 (2015) 2886–2889, https://doi.org/10.1039/C4CC07836E.
[71] N. Durán, C.P. Silveira, M. Durán, D.S.T. Martinez, Silver nanoparticle protein corona and toxicity: a mini-review, Silver nanoparticle protein corona and toxicity: a mini-review, J. Nanobiotechnol. 13 (2015) 1–17, https://doi.org/10.1186/s12951-015-0114-4.
[72] Q.L. Feng, J. Wu, G.Q. Chen, F.Z. Cui, T.N. Kim, J.O. Kim, A mechanistic study of the antibacterial effect of silver ions on Escherichia coli and Staphylococcus aureus, J. Biomed. Mater. Res. 52 (2000) 662–668, https://doi.org/10.1002/1097-4636(20001215)52:4%3C662::AID-JBM10%3E3.0.CO;2-3.
[73] S. Pal, Y.K. Tak, J.M. Song, Does the antibacterial activity of silver nanoparticles depend on the shape of the nanoparticle? a study of the gram-negative bacterium Escherichia coli, Appl. Environ. Microbiol. 73 (2007) 1712–1720, https://doi.org/10.1128/AEM.02218-06.
[74] P. Singh, S. Pandit, C. Jers, A.S. Joshi, J. Garnæs, I. Mijakovic, Silver nanoparticles produced from Cedecea sp. exhibit antibioflm activity and remarkable stability, Scient. Rep. 11 (2021) 1–13, https://doi.org/10.1038/s41598-021-92006-4.
[75] Y. Hong, D.G. Brown, Cell surface acid–base properties of Escherichia coli and Bacillus brevis and variation as a function of growth phase, nitrogen source and C: N ratio, Colloids Surf. B: Biointerfaces 50 (2006) 112–119, https://doi.org/10.1016/j.colsurfb.2006.05.001.

[76] A.S. Joshi, P. Singh, I. Mijakovic, Interactions of Gold and Silver nanoparticles with bacterial biofilms: molecular interactions behind inhibition and resistance, Int. J. Mol. Sci. 21 (2020) 7658, https://doi.org/10.3390/ijms21207658.
[77] J.L. Markley, T.A. Wencewicz, Tetracycline-inactivating enzymes, Front. Microbiol. 9 (2018) 1058, https://doi.org/10.3389/fmicb.2018.01058.
[78] K.C. Popat, M. Eltgroth, T.J. LaTempa, C.A. Grimes, T.A. Desai, Decreased Staphylococcus epidermis adhesion and increased osteoblast functionality on antibiotic-loaded titania nanotubes, Biomaterials 28 (2007) 4880–4888, https://doi.org/10.1016/j.biomaterials.2007.07.037.
[79] H.-J. Kang, D.J. Kim, S.-J. Park, J.-B. Yoo, Y.S. Ryu, Controlled drug release using nanoporous anodic aluminum oxide on stent, Thin Solid Films 515 (2007) 5184–5187, https://doi.org/10.1016/j.tsf.2006.10.029.
[80] P. Kortesuo, M. Ahola, S. Karlsson, I. Kangasniemi, A. Yli-Urpo, J. Kiesvaara, Silica xerogel as an implantable carrier for controlled drug delivery-evaluation of drug distribution and tissue effects after implantation, Biomaterials 21 (2000) 193–198, https://doi.org/10.1016/S0142-9612(99)00148-9.
[81] S. Radin, P. Ducheyne, T. Kamplain, B.H. Tan, Silica sol-gel for the controlled release of antibiotics. I. Synthesis, characterization, and in vitro release, J. Biomed. Mater. Res. 57 (2001) 313–320, https://doi.org/10.1002/1097-4636(200111)57:2%3C313::AID-JBM1173%3E3.0.CO;2-E.
[82] P. Gao, X. Nie, M. Zou, Y. Shi, G. Cheng, Recent advances in materials for extended-release antibiotic delivery system, J. Antibiot. 64 (2011) 625–634, https://doi.org/10.1038/ja.2011.58.
[83] T.Y. Liao, A. Biesiekierski, C.C. Berndt, P.C. King, E.P. Ivanova, H. Thissen, P. Kingshott, Multifunctional cold spray coatings for biological and biomedical applications: a review, Prog. Surf. Sci. (2022), 100654, https://doi.org/10.1016/j.progsurf.2022.100654.
[84] S.E. Yakhlifi, V. Ball, Polydopamine as a stable and functional nanomaterial, Colloids Surf. B: Biointerfaces 186 (2020), 110719, https://doi.org/10.1016/j.colsurfb.2019.110719.
[85] I.S. Kwon, C.J. Bettinger, Polydopamine nanostructures as biomaterials for medical applications, J. Mater. Chem. B 6 (2018) 6895–6903, https://doi.org/10.1039/C8TB02310G.
[86] R. Nordström, M. Malmsten, Delivery systems for antimicrobial peptides, Adv. Colloid Interface Sci. 242 (2017) 17–34, https://doi.org/10.1016/j.cis.2017.01.005.
[87] F. Geyer, M. D'Acunzi, C.-Y. Yang, M. Müller, P. Baumli, A. Kaltbeitzel, V. Mailänder, N. Encinas, D. Vollmer, H.-J. Butt, How to coat the inside of narrow and long tubes with a super-liquid-repellent layer - a promising candidate for antibacterial catheters, Adv. Mater. 31 (2019) 1801324, https://doi.org/10.1002/adma.201801324.